Original paper

Simulation and experimental validation of a prototype electron beam linear accelerator for preclinical studies

Pierre Lansonneur[a,*], Vincent Favaudon[b], Sophie Heinrich[c], Charles Fouillade[a,b], Pierre Verrelle[a,d], Ludovic De Marzi[a,b]

[a] Institut Curie, PSL Research University, Radiation Oncology Department, Proton Therapy Centre, Centre Universitaire, 91898 Orsay, France
[b] Institut Curie, University Paris Saclay, PSL Research University, Inserm U 1021-CNRS UMR 3347, Centre Universitaire, 91405 Orsay, France
[c] Institut Curie, RadeXp Platform, Centre Universitaire, 91405 Orsay, France
[d] Institut Curie, PSL Research University, Inserm U 1196-CNRS UMR 9187, Centre Universitaire, 91405 Orsay, France

ARTICLE INFO

ABSTRACT

Purpose: Measurements and Monte-Carlo simulations were carried out to model the dose distribution of a prototype electron beam linear accelerator (Kinetron LINAC) to determine the dose to organs in small animal irradiations experiments. Dose distributions were simulated using the GATE8.0/Geant4.10.3 Monte-Carlo platform, and measured in air and solid water phantoms using a commercial scintillating screen detector and new EBT-XD Gafchromic films.

Methods: The LINAC is able to produce 4.5 MeV electron beams at dose-rates ranging from Gy/min to thousands of Gy/s, and is used to study the radiobiological effects of very-high dose-rates that have been shown to protect normal tissues from radiation toxicity. Numerical simulations and experimental dosimetric characterisation of this electron accelerator were performed with the Monte-Carlo toolkit and various detectors. Absolute dose distributions in solid water were measured and compared with simulations. Realistic electron irradiation conditions were simulated in voxelised mice CT images. 3D dose distributions and dose-volume histograms in lungs of mice were simulated and analyzed.

Results: Measured and calculated depth-dose profiles for several beam configurations (energy and dose-rate) were compared. Beam emittance was validated by comparing measured and calculated beam sizes along the central axis in air: the deviation for all conditions was less than 1 mm. A good agreement was obtained between experimental dose distributions and the results obtained with simulations ($< 2\%$ dose differences for lateral and depth-dose profiles).

Conclusions: The method presented here, relying on few free parameters, can be adapted to very-high dose-rate electron irradiation to support the analysis of preclinical research experiments.

1. Introduction

Normal tissue protection from radiation-induced toxicity is a major concern in radiation therapy, and the radiobiological effectiveness of irradiation is highly dependent on dose and dose-rate. In particular, some elements indicate that the radiobiological response of tissues to very short or pulsed irradiations may be poorly elucidated. Recent *in vivo* investigations have shown that very-high dose-rate (FLASH) irradiation with electrons was less harmful for healthy tissues (lungs) in mice, but just as effective as conventional dose-rate gamma rays in terms of tumour growth inhibition [1]. Similar protection of normal tissue in a FLASH experiment has also been recently demonstrated in brain [2]. This sparing effect on healthy tissues, without compromising the anticancer effect, would open up extremely interesting prospects in clinical radiation oncology. The emergence of a new generation of particle therapy facilities (very-high energy electron beams, laser-based accelerators [3–5]) is also leading to the use of instantaneous dose-rates or doses-per-pulse up to several orders of magnitude greater than those produced by conventional radiation sources. In order to assess the dose distributions received by small animals irradiated under FLASH conditions, and to create a predictive dosimetry tool, we hereby describe the Monte-Carlo simulation and validation of the 4.5 MeV electron irradiation facility described in [1]. Such irradiators are gaining increasing attention following the demonstration of the FLASH sparing

---

* Corresponding author.
  E-mail address: kinetron_simulation@curie.fr (P. Lansonneur).

effect. It is also noteworthy that clinical LINACs can be turned into FLASH irradiators after simple modifications, thus paving the way to human treatments ([6,7]).

Ionisation chambers, recommended in many clinical practice guidelines, are the cornerstone of reference dosimetry in radiation therapy. However, for pulsed radiation with high dose-per-pulse (more than 5 mGy par pulse), incomplete charge collection due to re-combination, space charge and ion drift effects requires the use of complex non-linear saturation correction factors. Current methods used for dosimetry at conventional dose-rates function poorly at pulsed very-high dose-rates [8,9]. Dosimetric measurement is also a common issue in the case of very small field electron beams, such as those used for preclinical investigations [10]. An alternative is to use chemical dosi-meters operating at sub-microsecond timescales, such as those used in pulsed electron radiolysis and based on the formation of methylvio-logen radicals ([11,12]) or radiochromic films [13]. Radiochromic films are extensively used in electron beam dosimetry because of their low dose-rate and energy dependence [8,14,15]. To obtain parameterisation and validation of our model, we therefore used EBT-XD Gafchromic films and a scintillating screen coupled to a CCD camera for relative dosimetry of FLASH fields, cross-calibrated to reference dosimetry using an ionisation chamber to measure the absolute absorbed dose under conventional dose-rate conditions.

2. Methods and materials

2.1. LINAC specifications

FLASH irradiation was performed using the linear electron accel-erator (Kinetron LINAC) from CGR-MeV described in [1,16]. This ac-celerator provides a beam with 4.5 MeV nominal energy that can be operated according to two modes: a conventional irradiation mode (CONV), in which the mean dose-rate is set below 0.03 Gy/s, and a FLASH irradiation mode, in which typical instantaneous dose-rates up to 2×10^7 Gy/s can be achieved. Time structures of the pulses for the two modes are listed in Table 1. The machine also allows the possibility to tune the beam energy between 4 and 5 MeV by setting the magnetron voltage ("DQing" parameter). The Kinetron accelerating guide is pow-ered by a magnetron (3-GHz band, 2.5 MW peak power). The triode electron gun (11 kV accelerating potential) allows easy and reliable instant adjustment of beam current (10–250 mA) and pulse width (0.05–2.7 ps). The pulse-to-pulse reproducibility obtained is better than 5% [16].

As depicted in Fig. 1, two collimators made of 22 mm thick graphite are used to delimit the irradiation field, and protect the animals from whole-body exposure to radiation [1]. Time-resolved monitoring of the electron fluence is performed by measuring the charges collected in the first graphite collimator, electrically isolated by a high density poly-ethylene insulator. This plastic insulator is placed between the source and the first graphite collimator to allow real-time measurement of the beam current. The second graphite collimator is located 35 mm in front of the mouse with an 18×26 mm^2 rectangular aperture (for lung ir-radiation). The distance between the mouse and the electron source is 500 mm.

2.2. Monte Carlo modelling

Monte Carlo simulations of photon irradiators have been extensively explored due to growing interests in radiosurgery over the last 40 years [17]. However, only few studies have been published about the mod-elling of electron LINAC for small animals [18,19]. Simulations using the Gate 8.0 – Geant 4.10.3 Monte-Carlo platform [20,21] were per-formed to model the dose distribution of the beam and treatment head accelerator along the beamline. The physics builder set "em-standard_opt3" was used for electromagnetic interactions. The beam-line components, such as the primary source, the insulator and the collimators, were modelled. The uncertainty was defined as the average statistical uncertainty in voxels with a dose greater than 90% of the maximum dose and was estimated from the square root of the average variance of the voxels. A total of 10^9 electron histories were simulated for each setup such that the relative statistical uncertainty was less than 1%. Simulations were run on a multiprocessor Linux cluster (64 bit architecture, 16 cores). The range cut for all particles was set to 0.5 mm in the mouse volume, corresponding to a production threshold of ap-proximately 200 keV for electrons. The dose scoring grid resolution was $0.5 \times 0.5 \times 0.5$ mm^3. All other parameters used default options.

The source was modelled in the simulation by a planar disk with radius r_S oriented towards the z axis. It delivers an electron beam with an energy E and an energy spread σ_E. Beam divergence is modelled by a Gaussian distribution with an angular spread σ_Θ. Parameter optimisa-tion was performed using the non-linear least squares method provided by the python scipy environment [22] in order to obtain a good agreement between measurements and simulated data (see Table 2).

2.3. EBT-XD film dosimetry

For an experimental validation of MC simulations, we used a new type of radiochromic films (EBT-XD, Ashland Inc., USA). The sensi-tivity, anisotropy and stability of this detector has been improved compared to previous models (eg EBT2-3), making it a good candidate for FLASH relative dosimetry [23]. Absolute dose-response of the EBT-XD Gafchromic films up to 40 Gy was assessed by cross-calibrating the optical densities of a series of films with an ionisation chamber cali-brated in conventional mode.

The PPC05 parallel-plate ionisation chamber (IBA dosimetry, Germany) was used for absorbed dose-to-water determination, ac-cording to the IAEA TRS 398 recommendations for electron beam do-simetry. The absorbed dose-to-water was measured with the centre of an 8 cm diameter beam, in a water phantom located 78 cm away from the first graphite collimator. Polarity and recombination effects lower than 2% were observed with this chamber, and a beam quality cor-rection factor k_Q of 0.936 was used, as measured by [24].

In order to compare the dose profiles measured by EBT-XD dosi-metry with the ionisation chamber, a calibration curve was then per-formed for conversion of net optical density (netOD) to dose. The films were scanned 36 h after exposure with an EPSON Expression 10000XL scanner with no corrections applied to the image, while keeping the film angular orientation constant. To avoid discrepancies, films from the same batch (lot N°. 08021701) were used. The pixel values PV_{unexp} and PV_{exp} of the unexposed films and films exposed to irradiation were then averaged over three independent measurements in order to com-pute the net optical densities (netOD) in each channel (R, G and B):

$$netOD = log_{10}\left(\frac{\langle PV_{unexp} \rangle}{\langle PV_{exp} \rangle}\right) \tag{1}$$

For each channel, the calibration curve was then fitted by the ex-pression:

$$D = a \cdot netOD + b \cdot netOD^c \tag{2}$$

as proposed in reference [25] for EBT3 films, with D being the dose

Table 1
Beam pulse structure in FLASH and conventional (CONV) mode.

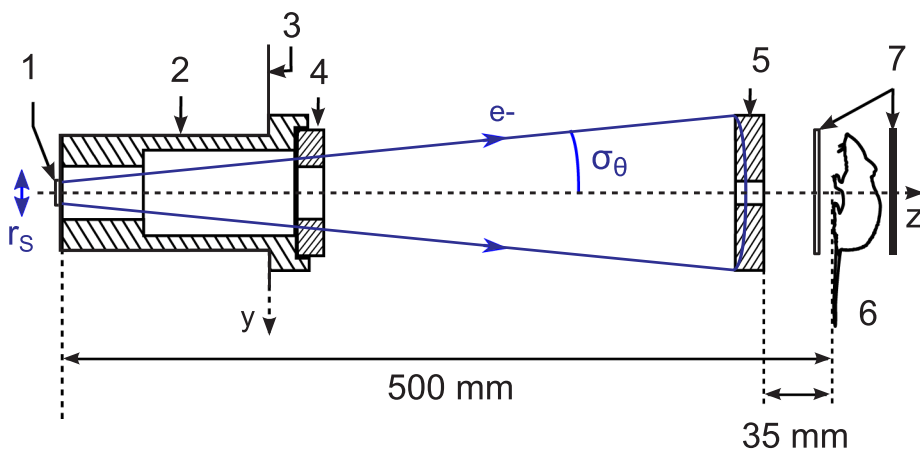|	FLASH mode	CONV mode
Energy	4–5 MeV	4–5 MeV
Pulse duration	0.1–2.2 μs	3 μs
Repetition rate	10–200 Hz	10–200 Hz
Dose per pulse	1 Gy	1 mGy

Fig. 1. Schematic view of the setup used for mice irradiation under FLASH conditions. 1, electron source. 2, high density polyethylene insulator. 3, LINAC front face. 4, primary graphite collimator (22 mm thick, 40 mm in diameter aperture). 5, 120×120 mm secondary graphite collimator (18×26 mm^2 rectangular aperture). 6, position of irradiated mice. 7, EBT-XD films used to measure the dose distribution downstream and upstream from the mouse.

Table 2
Experimental configurations used to set the beam source parameters.

| Measurement	Dosimetric device	Parameter investigated
Beam profile	LYNX, EBT-XD	r_S, σ_Θ
Depth-dose distribution (FLASH)	EBT-XD	E, σ_E (FLASH)
Depth-dose distribution (CONV)	Ionisation chamber	E, σ_E (CONV)

determined from the ionisation chamber reading and a, b and c the fitting parameters. Parameter optimisation was performed using the non-linear least squares method provided by the python scipy environment [22].

2.4. Depth-dose distributions

Schematic view of the setup used to measure the depth-dose distributions in conventional and FLASH modes is shown in Fig. 1.1 left and right, respectively.

2.4.1. Conventional dose-rate (CONV)

To measure the depth-dose profiles under conventional conditions, a 50 V voltage was applied to the electron gun grid and the dose was delivered by 3.5 µs pulses delivered at a 200 Hz repetition rate (2.1 mGy/pulse). Three measurements with a PPC05 chamber placed inside a RW3 plastic phantom (IBA dosimetry, Germany) were averaged for each depth. In order to overcome potential small variations of fluence between measurements, the chamber reading was cross-referenced to independent reading of a small cylindrical chamber used as a reference monitoring chamber. A 1.76 mm offset corresponding to the front window of equivalent thickness (1 mm Shonka C552, density 1.76) was applied in order to take into account the effective point of measurement of the detector.
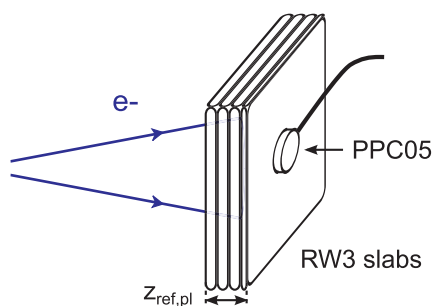
2.4.2. Very high dose-rate (FLASH)

In order to measure the depth-dose distribution under FLASH conditions (the use of an ionisation chamber is not suitable at such dose rates because of strong recombination effects), the EBT-XD film was placed horizontally between two RW3 slabs tightened with clamps and positioned 10 cm from the first collimator. To avoid underdosage artefacts at the entrance, an ultrasound transmission gel and another film sample were applied on the lateral side of the film at the entry surface of the phantom, as recommended by reference [26].

The dose was delivered at a dose-rate of 10^6 Gy/s (0.5 Gy pulses each delivered for 0.5 µs) at an expected energy of 5 MeV. The film was subsequently scanned with a resolution of 150 dpi and pixel values were converted to dose units using Eqs. (1) and (2) with the fit parameters of red channel.

2.5. Geometric properties

Beam profiles were measured with the LYNX (FIMEL, France), a 0.4 mm thick scintillator screen coupled to a charge-coupled device (CCD) camera. The field of view of the camera covers a 300×300 mm^2 (600×600 pixels) active area with an effective spatial resolution of 0.5 mm. The detector has been previously characterised (dose linearity, dose-rate independence, spatial resolution) and has been reported to be a good candidate for charged particle beam dosimetry [27]. 2D dose distributions at various positions along the beam axis as well were obtained with the detector in order to evaluate the divergence and size of the electron source.

2.6. Imaging, HU calibration and small animal irradiation

In order to assess the dose deposited in a digital phantom, CT images of a mouse were acquired on a Small Animal Radiation Research Platform (SARRP, Xstrahl) [28], using the parameters listed in Table 3. As small animal image acquisition and irradiation cannot be carried out using the same equipment, a mouse was anesthetised, immobilised in a
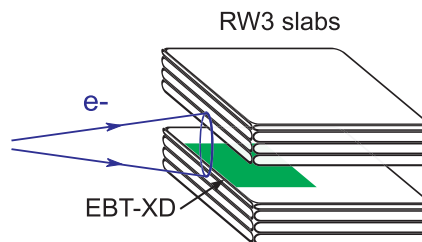

Fig. 1.1. Schematic view of the setup used to measure the depth-dose distributions in conventional (left) and FLASH modes (right). Details are given in the text.

Table 3
Parameters used for CBCT acquisition and reconstruction.

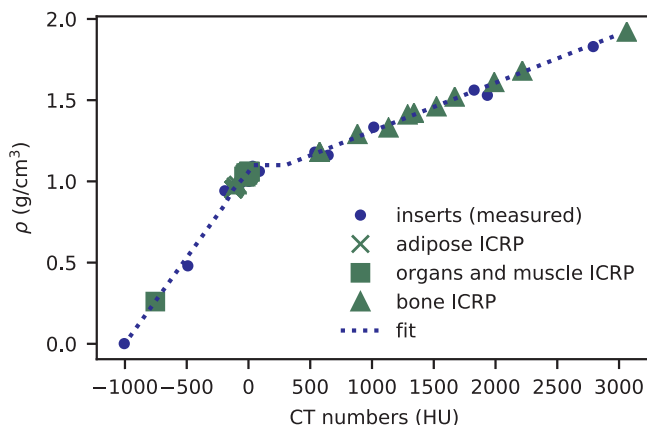| Energy	60 kV
Number of projections	720
Grid resolution	$0.245 \times 0.245 \times 0.245 \; mm^3$

Fig. 2. Calibration curve used to convert CT numbers into mass density, according to the method described in reference [29,30].

dorsal and vertical position, placed in a positioning device and kV-CBCT images were acquired. The stoichiometric calibration procedure described in [29] was used to determine the tissue substitute calibration curves of the SARRP, using a set of materials with known elemental composition and physical density close to those of tissue samples. This calibration was performed at the same time as mouse imaging, under equivalent geometrical conditions in order to mimic small animal scattering conditions. The calibration curve used to convert CT numbers into mass density is shown in Fig. 2. The images were then converted into a voxelised digital phantom using the "Hounsfield Material Generator" implemented in the GATE toolkit, according to the procedure described in references [29,30]. The small animal was then transferred to the irradiator facility, where irradiation was performed with films placed upstream and downstream from the mouse as shown in Fig. 1 (the lungs of the mice were exposed to a 17 Gy bilateral thorax irradiation). kV-CBCT images were acquired again at the end of the irradiation to check for consistency in the animal position.

3. Results

3.1. Dose-response curves of EBT-XD films

The dose plotted as a function of the optical density of the films is shown in Fig. 3, together with the fitting curve for a 5 MeV irradiation.

The fitting parameters corresponding to the dose-response curve shown in Fig. 3 are listed in Table 4.

3.2. Depth-dose distribution at conventional dose-rate (CONV)

The depth-dose distribution of electrons measured in the RW3 plastic phantom with a PPC05 ionisation chamber under conventional conditions (0.28 Gy/s) is shown in Fig. 4. The dose distributions for the 5 MeV electrons simulated for several energy spreads are shown in grey.

The distribution with the best fit to the data corresponds to a relative energy spread $\sigma_E/E = 0.27 \pm 0.03$ (k = 2).

3.3. Depth-dose distribution at very high dose-rate (FLASH)

Fig. 5.a shows the depth-dose distributions of 5 MeV electrons measured with EBT-XD films under FLASH conditions, compared to MC
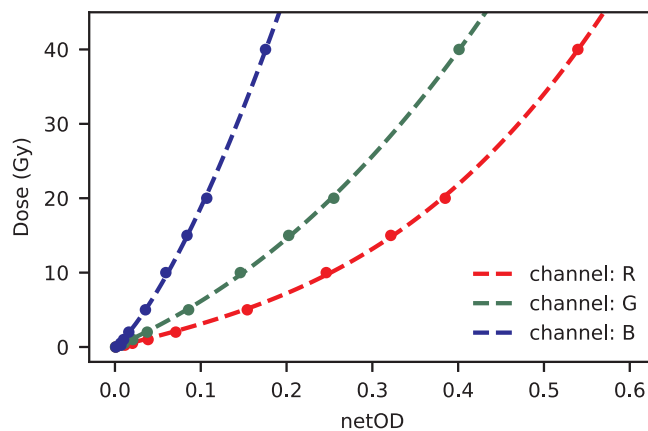

Fig. 3. Dose-response curves of EBT-XD films under conventional dose-rate irradiation with 5 MeV electrons. The optical density (netOD) is calculated using Eq. (1) as the average of three irradiations (points). Eq. (2) is used to fit the response curve in each channel (dotted lines).

Table 4
Fitting parameters for a coverage factor k = 2 and associated error (1 − σ) for the dose-response curve shown in Fig. 3. The blue channel presented the largest error and was not selected for dosimetric purposes in this study.

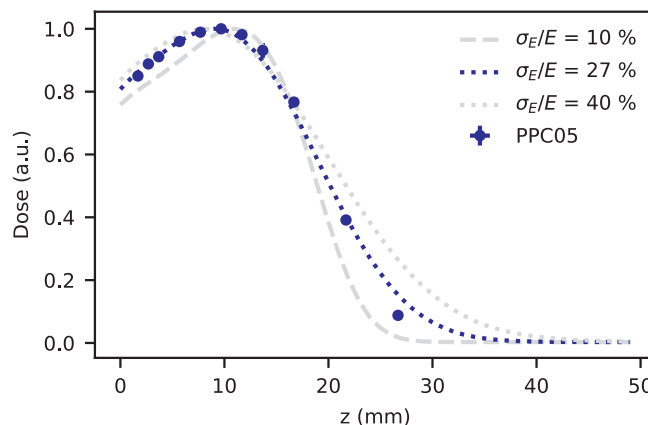| Channel	a (k = 2)	b (k = 2)	c (k = 2)
R	29.2 ± 1.7	145 ± 8	2.9 ± 0.14
G	53.5 ± 3.7	145 ± 13	2.3 ± 0.2
B	83.8 ± 35.0	395 ± 46	1.6 ± 0.2

Fig. 4. Depth-dose distribution of electrons measured in a plastic phantom with a PPC05 ionisation chamber under conventional conditions. The dose distributions of 5 MeV electrons simulated for different energy spreads are shown in grey.

simulations. It is noteworthy that the experimentally measured energy was consistent with the expected energy selected from the LINAC. The distribution with the best fit to the data corresponds to a relative energy spread $\sigma_E/E = 0.06 \pm 0.01$ (k = 2). Monte-Carlo simulation was validated by comparing an independent depth-dose profile (measured for 4 MeV set on the machine) with the output of the simulation. As shown in Fig. 5.b, a good agreement ($\sigma_E/E = 0.06 \pm 0.03$, k = 2) was observed between the Monte-Carlo simulation and the experimental curve.

In order to specify the energy and energy spread in the simulation, the depth-dose distribution was simulated for various pairs of parameters (E, σ_E) and the distance to the experimental points (Chi-square) was then calculated for each pair, as shown in Fig. 6.a.
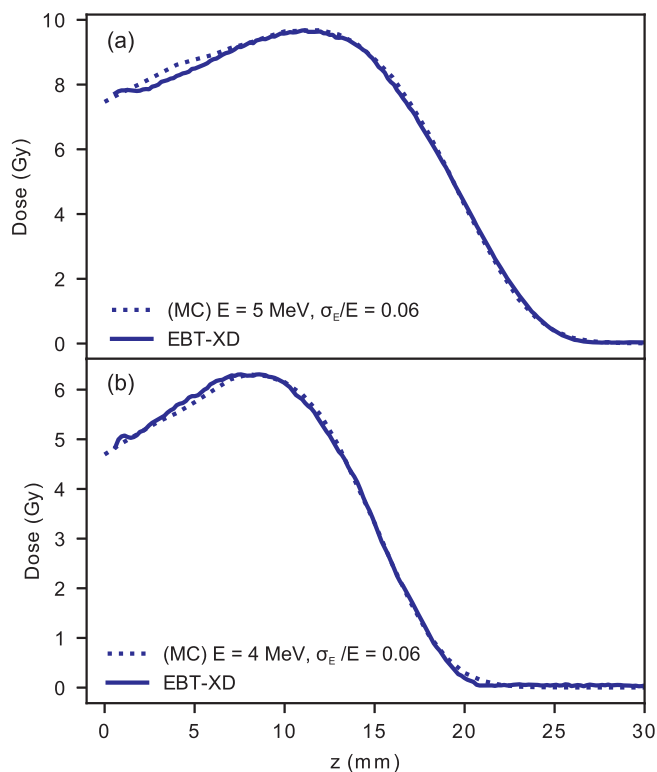
Fig. 5. Depth-dose distributions of 5 MeV (a) and 4 MeV (b) electrons measured with the EBT-XD films in a plastic phantom. The simulated (MC) distributions are plotted as a dotted line.

3.4. Geometric properties

Two free parameters may impact the electron beam size: the source radius and the angular spread at the exit of the source. In order to properly set their values in the simulation, beam sizes were measured at different locations inside the accelerator treatment head and along the beam axis. EBT-XD films were used for distances inside (between the source and the collimator) and close to the accelerator head, while the LYNX was used 0.9 m upstream from the collimator. Measurements therefore covered a region larger than 1 m in depth. The profiles obtained were fitted by a two-dimensional Gaussian distribution in both cases. The beam profile was simulated for various pairs of parameters (r_S, σ_Θ) and the chi square was then calculated for each pair as shown in Fig. 6.b.

The spreads measured are shown in Fig. 7 along with the fitted Monte-Carlo simulation for a source radius of 1.5 mm and an angular divergence of 13.5 deg.

The parameters (presenting the best fit with the data) used to model the electron LINAC are listed in Table 5.

3.5. Lung irradiation

In order to validate the Monte-Carlo simulation in a complex geometry (dose heterogeneity in the lungs) and to assess the dose distribution in a typical preclinical study, we then compared the dose distribution measured on the films with the output of the simulation.

The dose distributions measured on the films placed upstream and downstream from the mouse are shown in Figs. 8.a and 9.a, respectively. The MC-generated doses (Figs. 8.b and 9.b) were normalised to the dose measured on the film placed upstream and simulated and measured images for each film were compared by 2%/2 mm gamma index analysis [31] (Figs. 8.c and 9.c). For the film placed downstream from the mouse, on which large heterogeneities were observed, 90% of the pixels had a gamma index less than one.
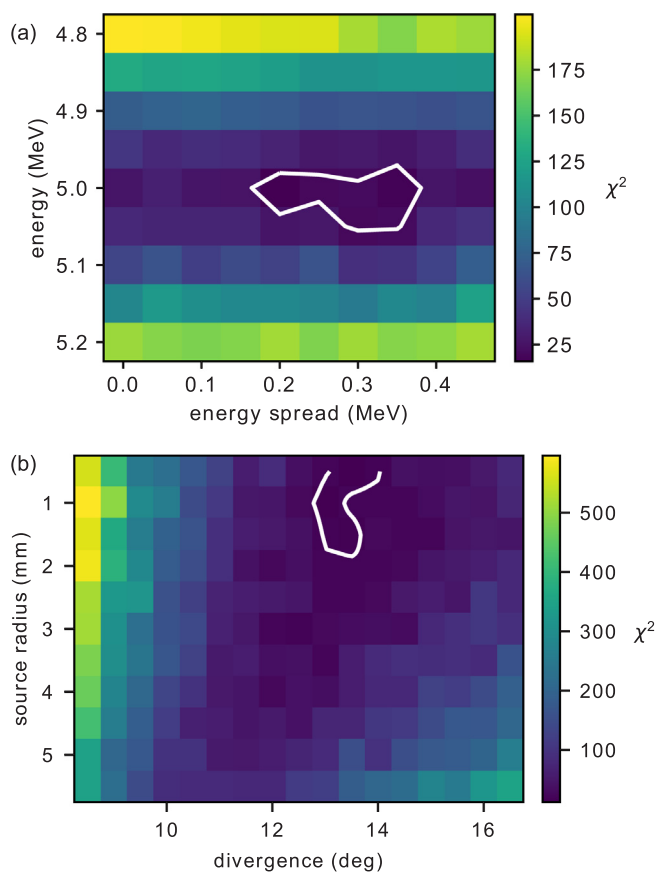

Fig. 6. Chi square calculated for different pairs of parameters. (a) Energy and energy spread. (b) Source radius and beam divergence. The white line delimits the 95% confidence interval.
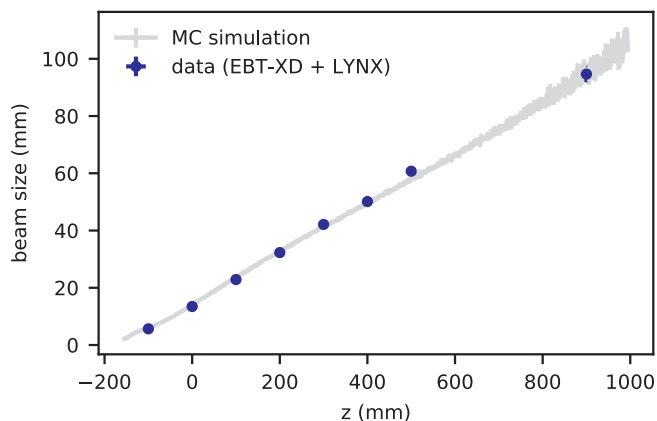

Fig. 7. Beam profile, measured at several distances along the beam axis with (blue points) EBT-XD films and scintillating screen and (grey line) simulated data for a source radius $r_S = 1.5$ mm and beam divergence $\sigma_\Theta = 13.5$ deg. (For interpretation of the references to colour in this figure legend, the reader is referred to the web version of this article.)

Table 5
Parameters used for source modelling together with their 95% confidence intervals (k = 2).

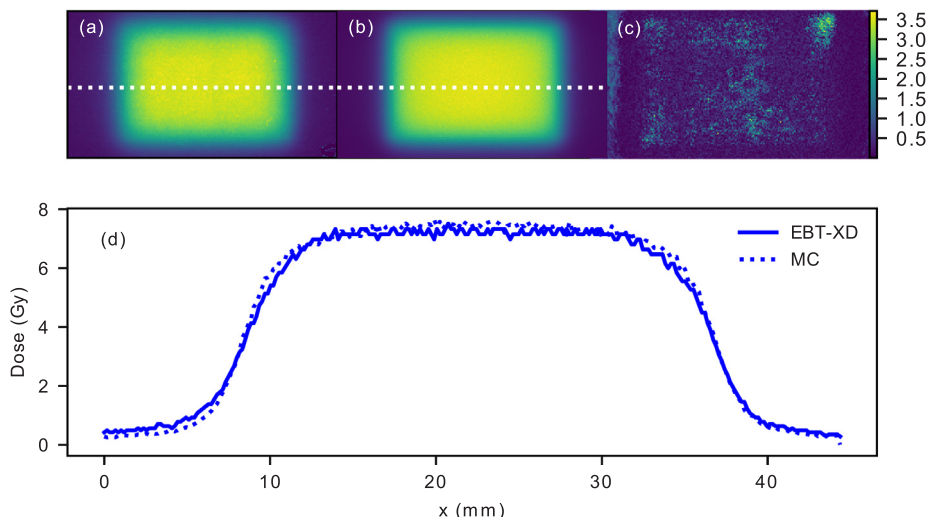|	
Energy	4.5 ± 0.05 MeV
Rel. energy spread	0.06 ± 0.01 (FLASH)
	0.27 ± 0.03 (CONV)
Angular spread	13.5 ± 1 deg
Source radius	1.5 ± 1 mm

Fig. 8. Dose distributions on the film placed in front of the mouse, measured with the EBT-XD film (a) andMC-generated (b). The 2%/2 mm gamma index is shown on the top-right corner (c). 91% of the pixels have a gamma indexless than one. The dose profiles measured along the white dotted line are shown on the bottom plot (d).

A good agreement was also observed between the two dose profiles measured along a median line (white dotted line), as shown in Figs. 8.c and 9.c. The remaining discrepancy between the two distributions can be attributed to small movements of the mouse (despite being anaesthetised) between the CBCT acquisition and irradiation.

Monte-Carlo simulations can be used as a predictive tool to infer the dose received by irradiated organs. The dose distribution obtained when irradiating mouse lungs with the setup described in Fig. 1 (corresponding to the experimental conditions of [1]) is shown in Fig. 10. We first compared the dose distributions obtained between the conventional and FLASH irradiation modes of the machine. No significant differences were observed between the two distributions. However, in both modes, the difference between the doses received by the two lungs, due to the presence of the heart, was especially visible in the transverse and coronal planes. The difference in mean dose visible on the dose-volume histograms (Fig. 10.c) was of the order of 10% (D_{50}).

4. Discussion

The simulation presented here only focused on small animal irradiation and 3D dose distributions with millimetric voxel sizes. Since other parameters were fixed by the geometry of the setup, the limited number of free parameters needed for the simulation allows this methodology to be applied to other electron irradiation facilities. The detailed characteristics of the beam may also serve as input to more sophisticated modelling, accounting for interactions of electrons at the cellular/molecular scale that require substantial calculation time. Simulating the processes at such a scale will undoubtedly be relevant for a better understanding of the FLASH sparing effect, and could be implemented in future work within the Monte-Carlo toolkit such as Geant4-DNA. The physicochemical and recombination processes occurring at high dose rates were not considered in this study, as these features are currently not fully covered in the Geant4 Monte Carlo simulation toolkit. Once validated, these features could expand the range of applications of the modelling presented here.

In Geant4, the range cut value is converted into threshold energies for each material and for each particle type (i.e. electron, positron and gamma), so that the particle with threshold energy stops (or is absorbed) after travelling the range cut distance [32]. In the case of small animal radiation therapy, dose distributions with electron production cuts between 10 μm and 1.0 m were compared [33], showing that a small overestimation in bone could be expected at the water/bone interfaces (partly due to the reduction of beam energy from MV to kV range for small animals). As no major discrepancies and no such
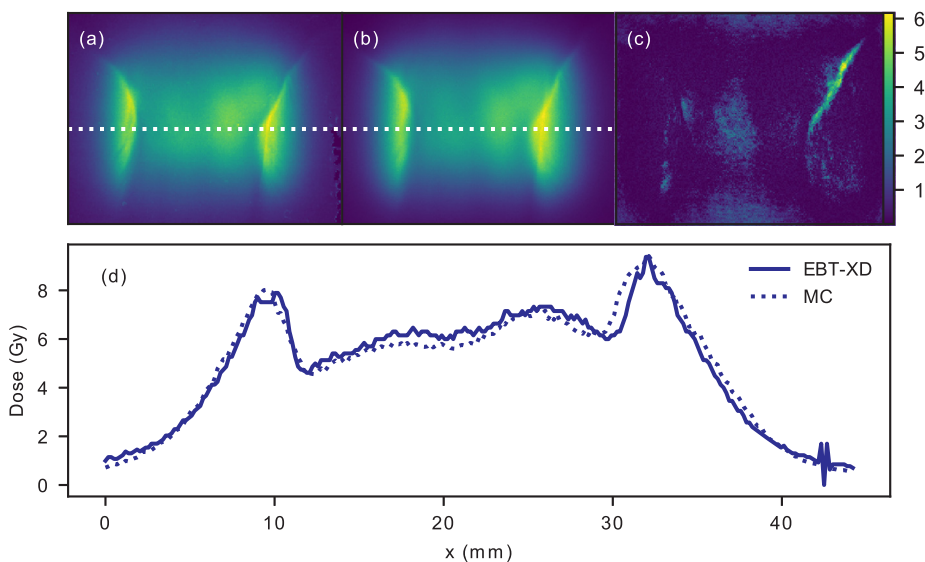

Fig. 9. Dose distributions on the film placed at the back of the mouse, measured with the EBT-XD film (a) and MC-generated (b). The 2%/2 mm gamma index is shown on the top-right corner (c). 90% of the pixels have a gamma index less than one. The dose profiles measured along the white dotted line are shown on the bottom plot (d).
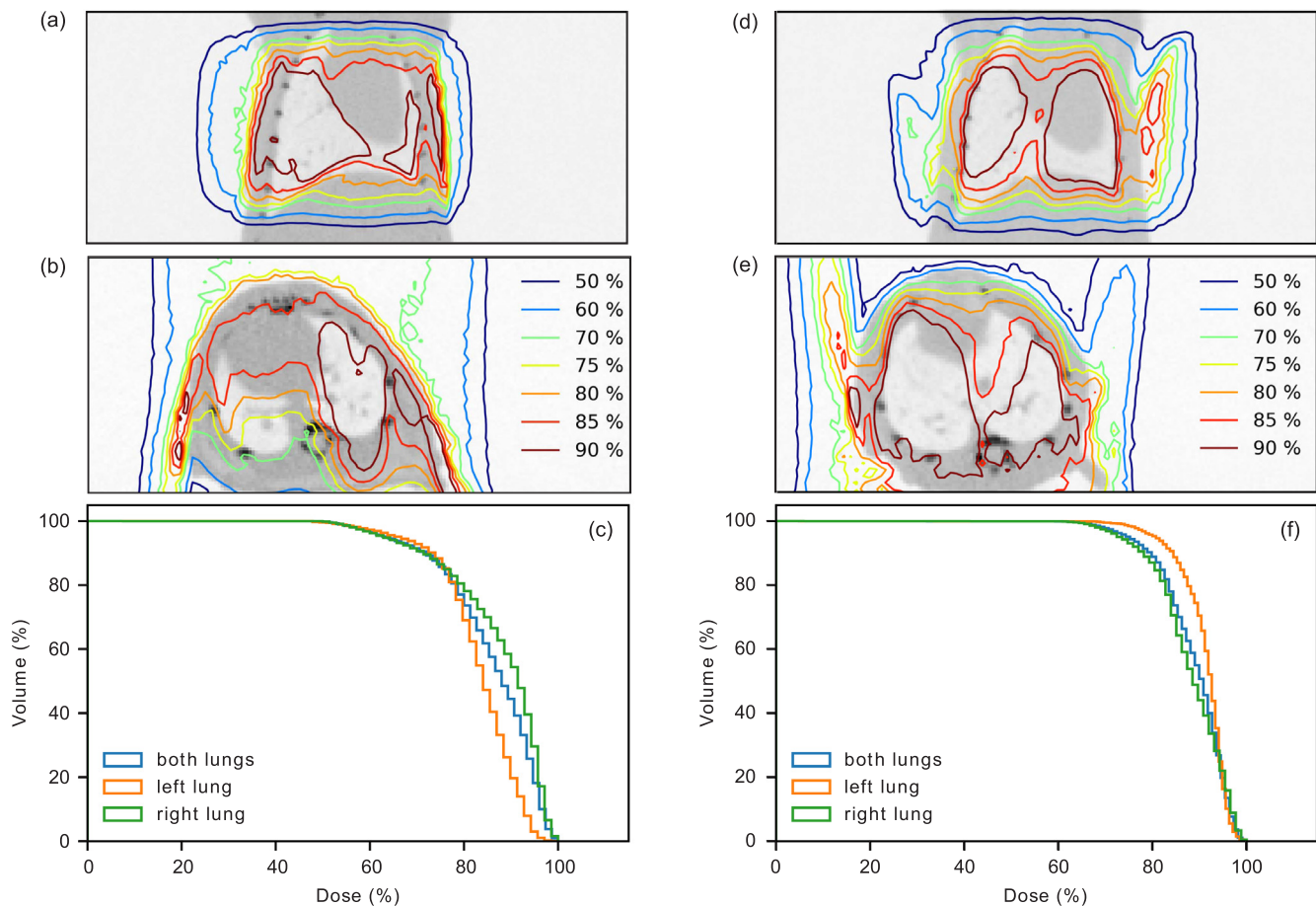
Fig. 10. Monte-Carlo generated dose distribution and dose-volume histograms for mouse lung irradiation. (a), (b) and (c) represents the output for irradiation from the thorax, while irradiation from the back is shown on panels (d), (e) and (f). When irradiating from the thorax, the electron beam first passes through the heart located in front of the left lung, thereby inducing a significant difference of the dose received by the two lungs. Irradiating from the back results in a more homogeneous dose distribution in both lungs.

differences at the water/lung interfaces or in homogeneous phantoms can be observed (same depth dose curves and mean doses within 2%) with the distributions presented in this paper, we decided to use a 0.5 mm setting (that corresponds to a threshold energy of ∼200 keV for electrons) in order to reduce computation times. The 2 mm criterion for gamma index analysis originates from the uncertainty of the positioning reproducibility of the mouse with our setup and respiratory motion (up to millimetres for sites within the thorax). Several references also describe mouse irradiators for which the distance-to-agreement acceptance criterion used for the gamma function is 3 mm [34] and discuss the implications of respiratory motion for small animal image-guided radiotherapy [35].

A significant difference in the dose received by the two lungs was observed when comparing irradiations with an anterior or posterior beam (Fig. 10, left and right panels, respectively). This difference, attributed to shielding by the heart or spine, is minimised by irradiating the mouse from the back. The dose distribution obtained in such a configuration is displayed in Fig. 10.d and e. Although the spine may induce a slight underdosage in the right lung, the dose distribution is more homogeneous. This observation is confirmed on the dose-volume histograms shown in Fig. 10.f. Relative doses D_{98} (corresponding to 98% irradiation of the left lung volume) of 52% and 66% were observed for anterior and posterior irradiation, respectively. The D_{50} dose difference between the two lungs also reached 10% for anterior irradiation and 5% for posterior irradiation, and these specific characteristics may be of interest when performing lung irradiation.

MC simulations are generally accepted to be the gold standard in terms of accurate dose calculation. However, due to the small number of validation cases, persistent uncertainties concerning material segmentation (all studies published to date have assigned human tissues data to animals due to lack of data on animal tissue compositions) and small animal positioning (particularly in the thorax with respiratory motion), major uncertainties persist and future studies are necessary to assess the accuracy of our simulation tool.

5. Conclusion

The field of very high dose-rate radiobiology is still in its infancy, but recent preclinical data showing a reduction of normal tissue toxicity, while still maintaining the same tumour control could dramatically transform the field of radiation oncology in the event of translation to clinical practice. Metrological and simulation tools are a prerequisite for the comparison of radiobiological effectiveness of different irradiation modalities. However, FLASH irradiation raises significant dosimetric challenges, and, to our knowledge, validation of Monte-Carlo modelling to describe this type of irradiation has never been reported. In this work, we modelled a prototype electron beam linear accelerator by comparing measurements and simulations, and computed the 3D dose distributions and dose-volume histograms in lungs on small animals. The results of this work, performed on a prototype electron linear accelerator, and more generally applicable to many particle accelerators, could support the analysis of radiobiological experiments for preclinical research with very high dose-rate electron beams.

6. Additional information and declarations

References

[1] Favaudon V, et al. Ultrahigh dose-rate FLASH irradiation increases the differential response between normal and tumor tissue in mice. Sci Transl Med 2014;6. 245: ra93.

[2] Montay-Gruel P, et al. Irradiation in a flash: unique sparing of memory in mice after whole brain irradiation with dose rates above 100 Gy/s. Radiother Oncol 2017;124:365–9.

[3] Sørensen BS, Vestergaard A, Overgaard J, et al. Dependence of cell survival on instantaneous dose rate of a linear accelerator. Radiother Oncol 2011;101(1):223–5.

[4] Auer S, Hable V, Greubel C, et al. Survival of tumor cells after proton irradiation with ultra-high dose rates. Radiother Oncol 2011;6:139.

[5] Rafat M, Bazalova M, Palma BA, et al. Impact of very rapid irradiation on clonogenic survival. Int J Radiat Oncol Biol Phys 2014;90:S790.

[6] Schuler E, Trovati S, King G, Lartey F, Rafat M, Villegas M, et al. Experimental platform for ultra-high dose rate FLASH irradiation of small animals using a clinical linear accelerator. Int J Radiat Oncol Biol Phys 2017;97:195–203.

[7] Lempart M, Blad B, Adrian G, Bäck S, Knöös T, Ceberg C, et al. Modifying a clinical linear accelerator for delivery of ultra-high dose rate irradiation. Radiother Oncol 2019. S0167-8140(19)30059-3.

[8] Karsch L, et al. Dose rate dependence for different dosimeters and detectors: TLD, OSL, EBT films, and diamond detectors. Med Phys 2012;39(5):2447–55.

[9] Burns DT, McEwen MR. Ion recombination corrections for the NACP parallel-plate chamber in a pulsed electron beam. Phys Med Biol 1998;43(8):2033.

[10] Chao TC. The evaluation of 6 and 18 MeV electron beams for small animal irradiation. Phys Med Biol 2009;54(19):5847–60.

[11] Das TN, Ghanty TK, Pal H. Reactions of methyl viologen dication (MV2 +) with H atoms in aqueous solution: mechanism derived from pulse radiolysis measurements and ab initio MO calculations. J Phys Chem A 2003;107:5998–6006.

[12] Katsumura Y. Ion beam pulse radiolysis study on intra-track reactions in aqueous solutions. Res Chem Intermediates 2001;27(4–5):333–41.

[13] Jaccard M, Petersson K, Buchillier T, et al. High dose-per-pulse electron beam dosimetry: usability and dose-rate independence of ebt3 gafchromic films. Med Phys 2017;44:725–35.

[14] Lechner W, et al. Characteristic of EBT-XD and EBT3 radiochromic film dosimetry for photon and proton beams. Phys Med Biol 2018;63(6).

[15] Sipilä P, et al. Gafchromic EBT3 film dosimetry in electron beams – energy dependence and improved film read-out. J Appl Clin Med Phys 2016;17(1):360–73.

[16] Favaudon V, Tourbe H, Houee-Levin C, Lhoste JM. Carboxyl radical induced cleavage of disulfide bonds in proteins. A gamma-ray and pulse radiolysis mechanistic investigation. Biochemistry 1990;29(49):10978–89.

[17] Verhaegen F, Seuntjens J. Monte Carlo modelling of external radiotherapy photon beams. Phys Med Biol 2003;48(21):R107.

[18] Kapur A, Ma CM, Mok EC, Findley DO, Boyer AL. Monte Carlo calculations of electron beam output factors for a medical linear accelerator. Phys Med Biol 1998;43(12):3479.

[19] Lee CC, Chen AM, Tung CJ, Chao TC. Monte Carlo simulation of small field electron beams for small animal irradiation. Radiat Meas 2011;46(12):2003–5.

[20] Jan S, et al. GATE – Geant4 application for tomographic emission: a simulation toolkit for PET and SPECT. Phys Med Biol 2004;49(19):4543–61.

[21] Sarrut D, et al. A review of the use and potential of the GATE Monte-Carlo code for radiation therapy and dosimetry applications. Med Phys 2014;41(6):064301.

[22] < http://www.scipy.org/ > , 2018 (accessed 2018-11-05).

[23] Khachonkham S, Dreindl R, Heilemann G, Lechner W, Fuchs H, Palmans H, et al. Characteristic of EBT-XD and EBT3 radiochromic film dosimetry for photon and proton beams. Phys Med Biol 2018;63(6):065007.

[24] Muir BR, Rogers DWO. Monte-Carlo calculations of electron beam quality conversion factors for several ion chamber types. Med Phys 2014;41:111701.

[25] Sorriaux J, et al. Evaluation of gafchromic EBT3 films characteristics in therapy photon, electron and proton beams. Phys Med 2013;29:599–606.

[26] Barouky JE, et al. Practical use of Gafchromic EBT films in electron beams for in-phantom dose distribution measurements and monitor units verification. Phys Med 2011;27(2):81–8.

[27] Russo S, Mirandola A, Molinelli S, et al. Characterization of a commercial scintillation detector for 2-D dosimetry in scanned proton and carbon ion beams. Phys Med 2017;34:48–54.

[28] Wong J, et al. A high resolution small animal radiation research platform (SARRP) with X-ray tomographic guidance capabilities. Int J Radiat Oncol Biol Phys 2008;71(5):1591–9.

[29] Schneider U, Pedroni E, Lomax A. The calibration of CT Hounsfield units for radiotherapy treatment planning. Phys Med Biol 1996;41(1):111.

[30] Schneider W, Bortfeld T, Schlegel W. Correlation between CT numbers and tissue parameters needed for Monte-Carlo simulations of clinical dose distributions. Phys Med Biol 2000;45(2):459.

[31] Low DA, et al. A technique for the quantitative evaluation of dose distributions. Med Phys 1998;25(5):656–61.

[32] Geant4 User's Guide for Application Developers, version: geant4 10.3 - 2016. < http://geant4-userdoc.web.cern.ch/geant4-userdoc/UsersGuides/ForApplicationDeveloper/BackupVersions/V10.3/fo/BookForAppliDev.pdf > .

[33] Smekens F, Létang JM, Noblet C, Chiavassa S, Delpon G, Freud N, et al. Split exponential track length estimator for Monte-Carlo simulations of small-animal radiation therapy. Phys Med Biol 2014;59:7703–15.

[34] Chow JCL, Leung MKK. Treatment planning for a small animal using Monte Carlo simulation. Med Phys 2007;34:4810.

[35] Hill MA, Vojnovic B. Implications of respiratory motion for small animal image-guided radiotherapy. Br J Radiol 2017;90:20160482.